Dendritic Growth and Structure of Undercooled Nickel Base Alloys*

by

M.C. Flemings and Y. Shiohara
Massachusetts Institute of Technology

ABSTRACT

The principal objectives of this overall investigation are to (1) study means (including microgravity) for obtaining high undercoolings in levitation melted droplets, and (2) study structures produced upon the solidification of these undercooled specimens.

Thermal measurements are made of the undercooling, and of the rapid recalescence, to develop an understanding of the solidification mechanism. Comparison of results is made with modelling studies. Characterization and metallographic work is done to gain an understanding of the relationship between rapid solidification variables and structures so produced. Undercoolings up to three hundred degrees centigrade have been obtained on earth, in spite of vigorous convection. The conduct of similar experiments under microgravity is expected to broaden the base of this information, and to extend the understanding of solidification behavior. Performing this experiment in space would permit near elimination of gravitational convection and induction stirring during undercooling and recalescence.

In ground based work to date, solidification of undercooled Ni-25wt%Sn alloy was observed by high-speed cinematography and results compared with optical temperature measurements.(1) Samples studied were rectangular in cross section, and were encased in glass. Cinematographic measurements were carried out on samples undercooled from 68 to 146K. These undercoolings compare with a temperature range of 199K from the equilibrium liquidus to the extrapolated equilibrium solidus. At all undercoolings studied, the high-speed photography revealed that solidification during the period of recalescence took place with a dendrite-like front moving across the sample surface. Spacings of the apparent "dendrites" were on the order of millimeters. The growth front moved at measured velocities ranging from 0.07 meters per second at 68K undercooling to 0.74 meters per second at 146K undercooling. These velocities agree well with results of calculations according to the model for dendrite growth of Lipton, Kurz, and Trivedi. It is concluded that the coarse structure observed comprises an array of very much finer, solute-controlled dendrites.

Also in ground based work, high-speed optical temperature measurements were made of the solidification behavior of levitated metal samples within a transparent glass medium.(2) Two undercooled Ni-Sn alloys were examined, one a hypoeutectic alloy and the other of eutectic composition. Measurements were carried out on samples at undercoolings up to 330K. Recalescence times for the 9 mm diameter samples studied decreased with increasing undercooling from the order of 1.0 second at 50K undercooling to less than 10^{-3} second for undercoolings greater than 200K. Both alloys recalesced smoothly to a maximum recalescence temperature at which the solid was at or near its equilibrium composition and equilibrium weight fraction. For the samples of hypoeutectic alloy that recalesced above the eutectic temperature, a second nucleation event occurred on cooling to the eutectic temperature. For samples which recalesced only to the eutectic temperature, no subsequent nucleation event occurred on cooling to the eutectic temperature. For samples which recalesced only to the eutectic temperature, no subsequent nucleation event was observed on cooling. It is inferred in this latter case that both the α and β phases were present at the end of recalescence. A solidification model is proposed for growth

* For presentations at the Science Review of Flight Experiments, Microgravity Science and Applications Division of NASA office of Space Science and Applications to be held at the George C. Marshall Space Flight Center, February 10, 1987.

and ripening of the dendrite structure during recalescence.

Microstructures of samples produced in ground based work were determined by optical metallography and by SEM, and microsegreation by electron microprobe measurements.[3] A gradual morphology change from dendritic to spherical was found with increasing undercooling, with the structure being fully spherical at about 180K undercooling. Dendrite element spacing was shown to be primarily determined by the ripening which occurred during cooling after recalsecence; this cooling took place in the range of 0.2 to 8 seconds, depending on sample size, undercooling and location in the sample. The extent of ripening in all samples must have been very large. For example, the calculated dendrite tip radii in samples undercooled 50 and 200K respectively were 0.2 and 0.017 micron. The radii of the dendrite elements observed were about 5 and 2 microns respectively. Hence the scale of the structure presumably increased about a factor of 25 at 50K undercooling and over 100 at the higher undercooling. Solute distribution and amounts and forms of eutectic were measured. The solidification model referred to above was employed to interpret results obtained.

A series of flight tests has been planned to conduct experiments similar to the ground based experiments described above. The main immediate objectives are to (1) evaluate containerless melting and solidification of nickel base alloys with and without glass coatings, (2) develop techniques for study of recalescence behavior, (3) develop an understanding of undercooling phenomena in a microgravity environment, and (4) develop an understanding of microstructures so produced. A hoped for ultimate objective of this work is to obtain higher undercoolings than are achievable in ground based experiments and to thereby produce and be able to study new structures of scientific and technological interest.

The Space Shuttle Columbia carried an alloy undercooled experiment in its STS 61-C mission in January 1986. A sample of Ni-32.5wt%Sn eutectic was melted and solidified under microgravity conditions. Because of unanticipated problems with the equipment, (clogging of cooling water lines), this undercooling experiment on the shuttle was cut short. Undercooling achieved was probably less than 30K. Interesting features observed on the solidified specimen included an apparent surface nucleation site, curved dendrites with non-orthogonal secondary dendrite arms, and dendrite fragments with extremely fine dendrite arm spacing (<0.5 micron) on the surface.

Additional experiments are projected for later flights to obtain higher undercoolings and improved data acquisitions, and to study the eutectic as well as the hypoeutectic Ni-Sn alloy. In addition, an experiment is planned with a different alloy which freezes over a much narrower solidification range than the Ni-25%Sn alloy. This could be Fe-Ni, Ni-Cu, or very dilute Ni-Sn.

Part I Dendrite Tip Velocity

The experimental apparatus used in this work consists of a high frequency levitation melter, an optical temperature measuring system with an overall response time of less than 6 microseconds, a data storage and manipulation system, and a high speed camera system with operating speeds up to 500 frames per second. For much of the work, metal samples were 9 mm in diameter, levitation melted within a glass slag. For portions of the work involving high speed photography, the glass slag was contained within a quartz tube of rectangular cross section, in order to obtain a sample with flat surfaces for better focusing of the camera as shown in Figure 1. The bulk of work conducted was on Ni-25% Sn alloy, a hypoeutectic alloy. Limited work was also conducted on the eutectic alloy Ni-32.5% Sn.

Undercoolings obtained in the work were up to 320 K. Temperature was measured before, during and after recalescence, and in a number of runs high speed motion photography was carried out during recalescence.

Figure 2 shows a series of eight photographs, taken 2 milliseconds apart, of recalescence of

a nickel-25wt% tin alloy which had been undercooled 131 K. The camera sees "dendrites" growing on the surface of the metal because of the temperature difference behind the growth front. The dendrites are significantly hotter than the bulk liquid into which they are growing. They appear darker on this negative photograph. Figure 3 is a drawing of the progression of the dendrites shown photographically in Figure 2, and Figure 4 is a plot of interface position vs. time of the growing dendrites. Curves a through c represent growing dendrite tips while curve e, progressing at a much slower rate, represents the thickening rate of one of the dendrites. A summary of data from a series of runs of growth velocity vs. undercooling is shown in Figure 5, and Figure 6 shows these same data (the black points) on another plot. Figure 6 also contains data points on dendrite tip velocity obtained from thermal measurement, as will be described in Part II below. Finally, it compares these data to three important dendrite growth models, that of Lipton, Kurtz and Trivedi (LKT), [5]; of Boettinger and Coriell (BC), [6]: and that of Lipton, Glicksman and Kurtz (LGK), [7].

Note that the agreement of our experiment with these theories is quite good. The most recent, and most precise, is the LKT model, although it differs little from the BC model for the range of parameters in this work. Figure 7 plots the various undercoolings at the dendrite tip vs. total undercooling, and this plot is helpful in understanding how the growth proceeds. For example, consider dendritic growth at a total bulk undercooling of 200 K. The dendrite tip is growing at a temperature of only about 6 K above the bulk liquid temperature; this is the amount of the thermal undercooling ΔT_α. The bulk of the undercooling, approximately 160 K, results from buildup of solute at the dendrite tip, ΔT_D, and the remainder of the undercooling, approximately 35 K, is accounted for by depression of the liquidus temperature from the curvature effect, ΔT_r. Figure 7 shows that for bulk undercoolings even to temperatures well below the equilibrium solidus, dendrite growth is controlled primarily by solute diffusion. It also shows that the dendrite tip temperature is not greatly different from the bulk liquid temperature. Hence the "dendrites" that we see by cinematography must, in fact, represent an isotherm somewhat back from the dendrite tip where recalescence has occurred to a point that there is a visible temperature difference.

Another result of the theory is plotted in Figure 8; that is, dendrite tip radius vs. bulk undercooling. This calculated radius is quite small, since it is controlled primarily by solute diffusion. It ranges from approximately 0.2 microns at 50 K undercooling to approximately 17 nanometers at 200 K undercooling. Yet the "dendrites" that we see by high speed cinematography are very much larger than this. These measured tip radii are also plotted in Figure 8, and it is seen that they are about three orders of magnitude larger than the calculated radii. The suggestion is clear - that what we see is a growth front morphology determined by thermal diffusion, whereas the actual growing dendrites themselves must be very much smaller, controlled primarily by solute diffusion.

Our schematic model of a growing dendrite to account for these observations is shown in Figure 9. The growth front proceeds into the bulk undercooled metal with a large thermally controlled, dendrite-like morphology, as sketched. Within these large dendrite features are growing very much smaller solute controlled dendrites, whose tip radius and growth behavior is described by analyses such as that of LKT. Recalescence behind the dendrite tip occurs very rapidly so that recalescence is substantially complete not far behind each growing tip. Some isotherm such as that sketched as T'_R is then the isotherm observed cinematographically.

Part II Recalescence Behavior

As indicated earlier, recalescence behavior was measured optically. The temperature measurement system consisted of a two-color pyrometer (Capintec Ratioscope III), a pair of matched amplifier circuits, and a digital storage oscilloscope (Nicolet, model 2090-III). The two silicon photocells of the pyrometer operate at narrow near-infrared wavelength bands centered at 0.81 and 0.95 microns. The response time of the temperature measurement system was less than 6 microseconds. A computer (Hewlett Packard, model 85) was interfaced to the oscilloscope for calculations.

Figure 10 shows two typical recalescence curves. There is first a period of "rapid recalescence," followed by a period of "slow recalescence." In the sample undercooled only 125 K there is finally seen a period of temperature decrease, due to heat extraction to the surroundings.

The time for the period of "rapid recalescence" ranges from fractions of milliseconds at high undercoolings to some seconds at low undercoolings (Fig. 11). With the model for dendritic growth described earlier in mind, we can use these thermal data to obtain a separate and confirming estimation of dendrite tip velocity. Assuming rapid recalescence progresses so quickly that it is nearly complete just behind the growing dendrite tip, then the time for rapid recalescence must represent the time for dendrites to sweep across the sample surface. Hence, dendrite tip velocity is given by something like the sample diameter divided by recalescence time. The thermally determined points for dendrite tip velocity in Figure 6 were calculated in this way.

The period of "slow recalescence" seen is dramatically slower than the period of rapid recalescence. It is so dramatically different that it leads one to suspect immediately a different mechanism is involved. Figure 12 shows recalescence of one sample plotted in a different way, as residual undercooling vs. time on a log scale. Note that the portion of this curve to the far right (portion representing the period of slow recalescence) plots as a straight line with a slope of -1/3. This result, and other results including metallography to be discussed later, is strongly suggestive that the period of slow recalescence is controlled by ripening of the dendritic structure which first forms.

The maximum recalescence temperature measured for a number of runs is plotted in Figure 13 vs. initial bulk undercooling. For undercoolings greater than about 100-120 K the data correspond closely to the assumption that, at the maximum recalescence temperature the liquid and solid phases are present at their equilibrium compositions and amounts. This result, at first surprising, is to be expected as a result of the extremely fine structures that form, and assuming ripening is occurring to a significant extent. Experimental results deviate significantly from the calculated results (based on simple adiabatic recalescence) at lower undercoolings. This, we believe, is due to the fact that recalescence at the lower undercoolings is not adiabatic, and significant heat extraction to the surrounding is occurring during the later stages of recalescence.

Thermal curves of samples following recalescence show the typical types of cooling curves observed in usual castings and ingots. That is, for the hypoeutectic alloy, when recalescence occurs above the eutectic temperature, the cooling curves show first formation of the primary phase alpha during cooling to the eutectic, and then nucleation and growth of the eutectic at the eutectic temperature, Figure 14.

Figure 15 summarizes our model for the solidification of these melts in terms of the "paths" of the liquid and solid compositions during recalescence. Consider a sample undercooled to a temperature T_N. Solute buildup in front of the dendrite tip results in a surface liquid composition given by the point A. The solid composition is then A' given according to the equilibrium partition ratio. Both A and A' are depressed from the equilibrium liquidus and solidus by ΔT_r, the depression of the equilibrium curves from the radius of curvature effect. Recalescence behind the dendrite tip is then limited by solute diffusion within the interdendritic regions and liquid and solid compositions at the interface move upwards during the period of rapid recalescence to the temperature T_R. Thereafter they rise more slowly to the equilibrium liquidus and solidus (assuming adiabatic recalescence). Finally, the temperatures fall due to heat extraction to the surroundings and the remaining solidification is as in usual castings and ingots.

Part III Structure and Microsegregation

Microstructure of undercooled nickel-25wt% alloy was found to exhibit a morphology transition from a typical dendritic structure at low undercoolings to a spherical, non-dendritic structure at high undercoolings, as can be seen in Figure 16. We believe the morphology changes seen with increasing undercooling result directly from the increasing ripening that occurs at the higher undercoolings. Many microstructural observations tend to qualitatively support this view. The existence of ripening can be seen in a simple way be examining microstructures at different locations within a given sample. Figure 17 shows a series of microstructures at different locations within a 9 mm diameter sample of the hypoeutectic alloy undercooled 324 K. Dendrite element spacing varies significantly from surface to center as a result of ripening, and experimental results agree well with simple calculations.

The explanation of the results obtained is that although cooling rate is essentially the same at

center and surface, the large amount of eutectic present results in a "local solidification time" that is much longer at the center than at the surface of the sample. The local solidification time is the sum of the time for solidification of the primary phase and for solidification of the eutectic. The time for eutectic solidification is the time for the eutectic solidification front to reach the given radial location; therefore, the local solidification time is dependent on the location. For the calculated results shown in Figure 17, the usual relationship of dendrite arm spacing and local solidification time, which is based on the ripening kinetics, was applied.

Quantitative measurement of solute concentration in the dendrites was made using electron microprobe analysis (EMPA). Typical profiles across dendrite arms are shown in Figures 18 and 19. Figure 18 shows a profile obtained from a region near the center of a sample undercooled 62K. The solute concentration increases radially outwards in the dendrite arm. Figure 19 is a profile obtained from a typical highly undercooled sample. This specimen, undercooled 324K, shows negligible segregation of solute in the spherical "dendrite element." The solute concentration in the spherical elements was about 19wt%Sn, and the composition of the second phases was 40wt%Sn. These are the compositions of the two phases at equilibrium at the eutectic temperature.

Minimum measured solute concentrations for a number of samples are plotted versus initial undercoolings in Figure 20 with calculated curves. The calculated curve #1 is based on a simple model assuming complete equilibrium of liquid and solid at the maximum recalescence temperature. Curve #2 makes this assumption and also assumes that liquid forming from remelting during recalescence is trapped with the growing dendrite arms.

The volume fraction of lamellar eutectic structure was observed to decrease with increasing undercooling, as may be seen qualitatively from the photographs of Figure 16. The measurements of volume fraction of lamellar eutectic structure were made by point counting. Figure 21 shows measurements of volume fraction of lamellar eutectic structure compared with calculated curves. Curve #1 and #2 are calculated on the same bases as the similarly numbered curves in Figure 21, referred to above.

The microstructure of the eutectic alloy is significantly affected by undercooling. In general, the microstructure of an undercooled eutectic sample consists of two distinguishable regions: normal lamellar eutectic and anomalous eutectic. Figure 22 shows structures for three Ni-32.5wt%Sn eutectic alloy samples with different initial undercoolings. At low undercoolings, the structure is largely lamellar eutectic (Fig 22[a]). At intermediate undercoolings, the structure is composed of the two regions (Fig. 22 [b]). In samples with high undercoolings (Fig. 22 [c]), lamellar eutectic can be observed only at high magnification. Figure 23 shows that the volume fraction of lamellar eutectic decreases with increasing initial undercooling.

Part IV Flight Experiment Performed

The Space Shuttle Columbia carried an Alloy Undercooling Experiment on its STS 61-C mission in January, 1986. The experiment was performed in the electromagnetic levitator (EML). A sample of Ni-32.5wt%Sn eutectic was melted and solidified under microgravity conditions. Because of unanticipated problems with the equipment, (clogging of cooling water lines), this undercooling experiment on the shuttle was cut short. The data of the temperature - time trace of the sample during heating, melting and solidification are shown in Figure 24. The data were obtained at a rate of 125 measurements per second using a pyrometer. The large amount of noise is due to insufficient isolation of the measurement circuit. The severe noise which occurred at the time of power cut-off is due to the operation of a motion picture camera. The noise caused difficulty in estimating the level of undercooling attained. This result with others including solidificaiton time measurement indicate that the specimen undercooling was probably less than 30K.

Metallographic examination of the specimen revealed an apparent nucleation site, shown in Figure 25(a). At low magnification, it can be seen that a large curved dendrite proceeds from this site. No other such obvious nucleation site was found on the surface of the specimen. A higher magnification photograph of the dendrite is shown in Figure 25(b). The secondary arms are not orthogonal to the primary branch. This curved dendrites (bending) is thought to be caused by thermal stress due to nonuniform heat flow and/or mechanical stresses due to convection

(Marangoni effect). Curved dendrites have not been observed on any samples in ground based experiments of this study.

Because the specimen attained only a small undercooling, the microstructure consists primarily of lamellar eutectic. Several patches of anomalous eutectic structure were also found, as shown in Figure 26. The fraction of anomalous eutectic in the cross-section of the flight specimen was measured at less than 10 percent, corresponding to initial undercooling of less than 30K (Figure 23). One type of feature, which was discovered, does not at first, seem consistent with the fact that the initial undercooling of the specimen was small. A number of dendritic fragments, such as that shown in Figure 27, were observed on the surface. The secondary arm spacing of this dendrite is less than 1 micron. The explanation of this observation must be that the fine spacing is due to decanting of the remaining liquid from the surface due to shrinkage during solidificaiton, so that little coarsening occurred.

Part V Projected Space Experiments and Objectives

Objectives and rationale for the flight experiments

On earth, we have achieved up to 320 K initial undercooling for Ni-25wt%Sn and Ni-32.5wt%Sn alloys. We hope to achieve higher undercoolings under microgravity conditions, since the higher power would not be needed to maintain levitation during cooling, and no gravitational convection due to difference of densities take place. A goal would be to attain the "hypercooling" regime, where comlete solidification would be achieved during recalescence. Amounts of "hypercooling" (which is an undercooling below the liquidus equal to the sum of equilibrium freezing temperature range and latent heat of fusion divided by specific heat) are about 500K for Ni-25wt%Sn and about 450K for Ni-1wt%Sn alloy.

If we can achieve these high undercoolings in space, the exciting opportunity would be made available to obtain, examine, and test new structures and phases in specimens much thicker than usual "splat-cooled" or other earth based rapidly solidified specimens. We would expect to obtain fully homogeneous, non-dendritic structures, and in some cases metastable phases.

On earth, rapid solidification can be attained and also practically used by rapid quenching such as melt spinning and gas atomization processes. In these processes, rapid solidification rate is gained by heat extraction to the surroundings, therefore, the obtainable materials are usually limited in size, generally less than 100 microns. In the proposed experiments herein, we could obtain rapidly solidified materials in relatively large sizes of 1 centimeter in diameter, since the heat to be extracted for solidificaiton would be extracted before the onset of solidification, provided "hypercooling" is achieved.

Space experiments now projected are to obtain higher undercoolings and improved data acquisition. An experiment is also planned with a different alloy which freezes over a much narrower solidification range than Ni-25wt%Sn. Lower undercooling would be required for the alloy closer to achieve "hypercooling". The alloy could be Fe-Ni, Ni-Cu, or very dilute Ni-Sn. The planned (proposed) shuttle experimental conditions are given in detail in Table 1.

Current ground based research work is providing the background for understanding solidification behavior and structures at high undercoolings. This work permits us to develop and predict parameters for space experiments, and to develop improved techniques for these space experiments.

REFERENCES

1. Y. Wu, T.J. Piccone, Y. Shiohara and M.C. Flemings, accepted for publication in Met. Trans. A (1987)
2. T.J. Piccone, Y. Wu, Y. Shiohara and M.C. Flemings, accepted for publication in Met. Trans. A (1987)
3. Y. Wu, T.J. Piccone, Y. Shiohara and M.C. Flemings, to be submitted for publication
4. T.J. Piccone, F.H. Harf, Y. Wu, Y. Shiohara, M.C. Flemings and E.A. Winsa, proceedings of MRS Fall Meeting Symposium (1986)

5. J. Lipton, W. Kurz and R. Trivedi, to be published in Acta. Met.
6. W.J. Boettinger and S. Coriell, proceedings of NATO Workshop on "Rapid Solidification Technologies", Castle of Theuren, FRG, (March 1985)
7. J. Lipton, M.E. Glicksman and W. Kurz, Mat. Sci. Eng., 65 (1984), 570

Table 1 Experimental conditions for projected space experiments

MATERIALS:

Alloy	Ni-25wt%Sn	T_L-T_S = 200 K	T_L = 1507 K
	Ni-1wt% Sn	= 8 K	= 1740 K
	Ni-5wt% Sn	= 65 K	= 1699 K
	Fe-25wt%Ni	= 16 K	= 1722 K
	Ni-10wt%Cu	= 11 K	= 1706 K

Glass

with and without glass coatings

Ferro-brand EG-0222 silicate glass

Pyrex-brand 7740 borosilicate glass

Size

Metal: 7 - 10 mm (in diameter)

Glass coating thickness: 0.3- 1.0 mm

HEATING: High frequency induction heating.

ATMOSPHERE: Inert gas (Ar, or He), Vacuum, and/or He-H_2 gas

"To avoid oxidation of the metal samples by direct exposure of the metal surface to the ambient atmosphere"

DATA ACQUISITION:

(a) Pyrometric temperature measurements

i) 125 data points/second for entire heating and cooling cycle,

ii) 2000 or more data points/second for approximately 30-40 seconds after power cut-off,

iii) Assured accuracy by use of a proper lens and two- or three-color pyrometer,

iv) Maximum noise should be under ± 5 K,

v) After calibration and smoothing, precision should be within ±5 K.

(b) Cinematography

In each cycle, the surface of the spherical specimen should be observed and cinematography will be made:

i) For 30-40 seconds at 16 frames/second after power cut-off, A much faster frame speed would be desirable.

ii) with 0.1 mm resolution or better at the specimen surface,

iii) with depth of field (in focus) larger than 2 mm in diameter for a sphere, and preferably larger than 5 mm.

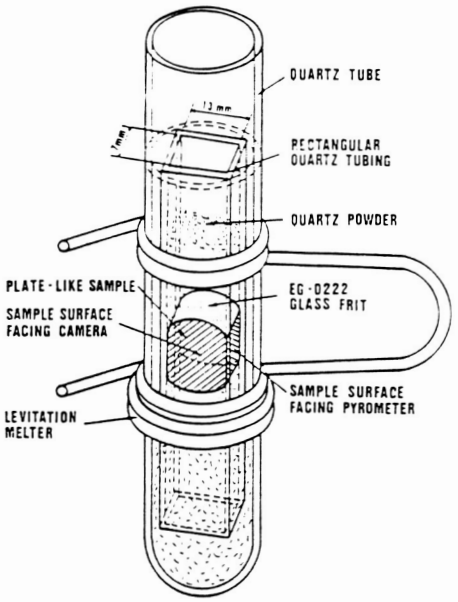

Figure 1. Sample assembly used for photographic measurements of growth behavior.

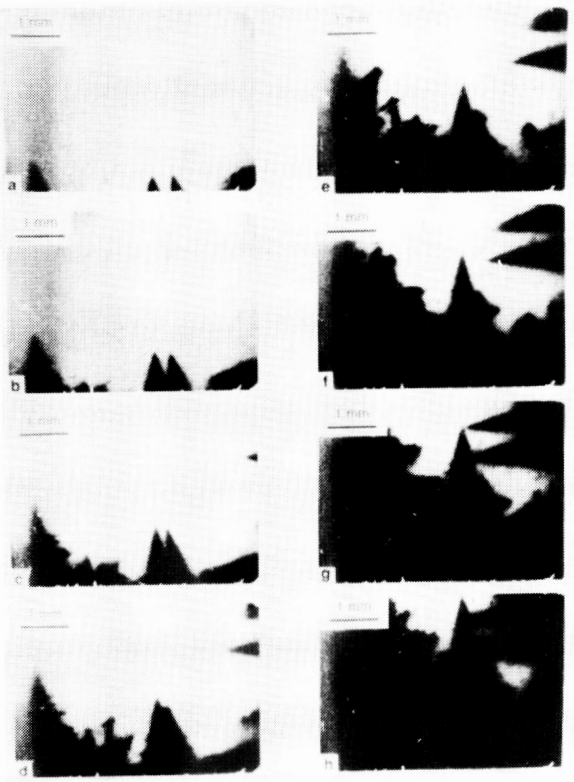

Figure 2. Eight photographs, taken 2 milliseconds apart, of recalescence of a Ni-25wt% Sn hypo-eutectic alloy sample undercooled by 131 K.

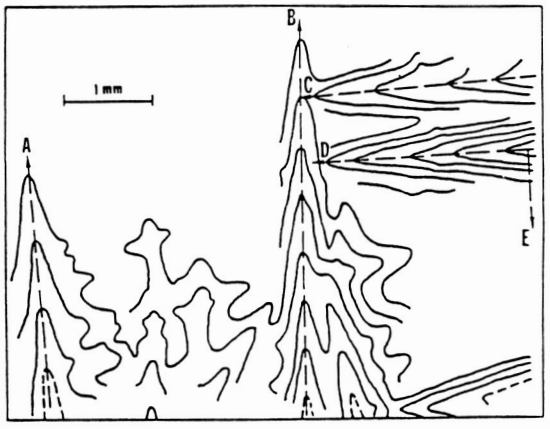

Figure 3. Drawings of the advancing solid-liquid interface of a Ni-25wt%Sn hypoeutectic alloy sample during recalescence. Undercooling is 131 K. The time interval between lines is milliseconds. Drawings were traced from photographic negatives.

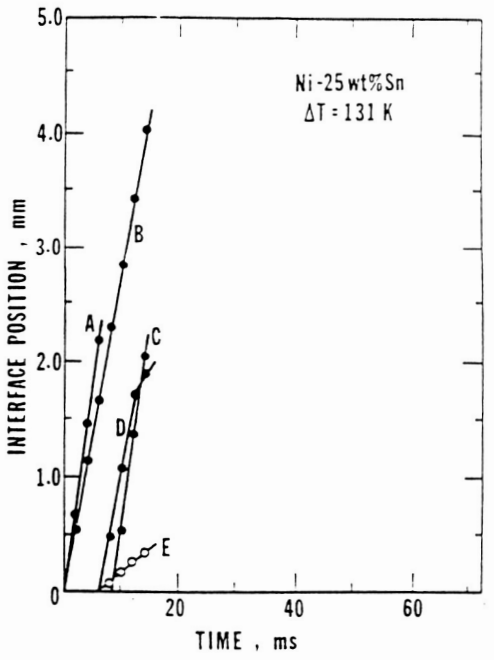

Figure 4. Movement of several parts of an advancing solid-liquid interface versus time for a Ni-25wt%Sn hypoeutectic alloy sample undercooled by 131 K. A, B, C, D, and E correspond to dendrites and directions shown in Figure 3.

C-6

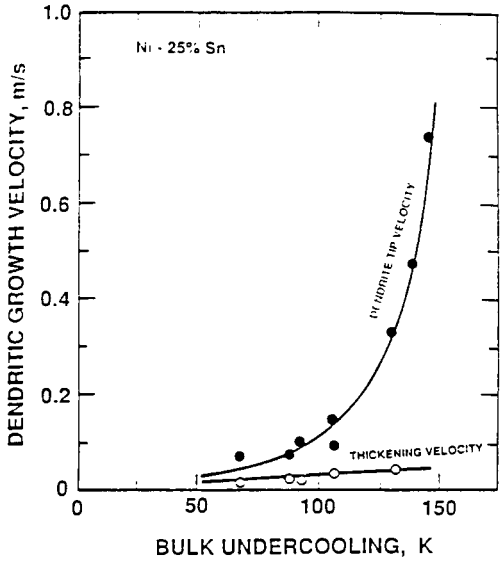

Figure 5. Dendrite tip velocity and dendrite thickening velocity versus initial undercooling for Ni-25wt%Sn alloy samples, measured by high-speed cinematography.

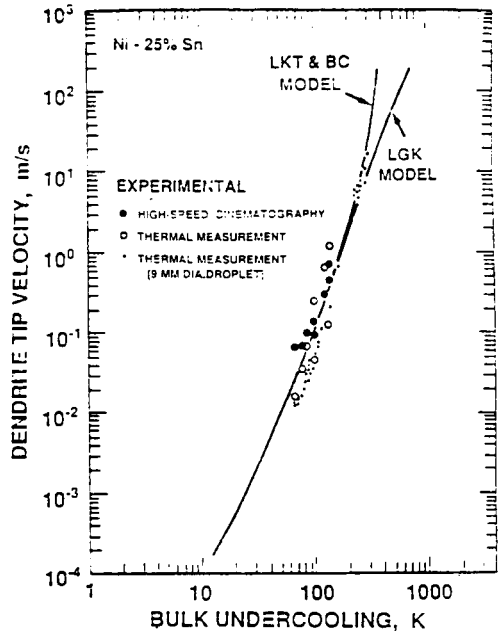

Figure 6. Dendrite tip velocity vs. bulk undercooling for Ni-25wt%Sn alloy. Experimental results and calculated curves based on the models developed by Lipton, Kurz, and Trivedi and Boettinger and Coriell (LKT-BC) and Lipton, Glicksman, and Kurz (LGK).

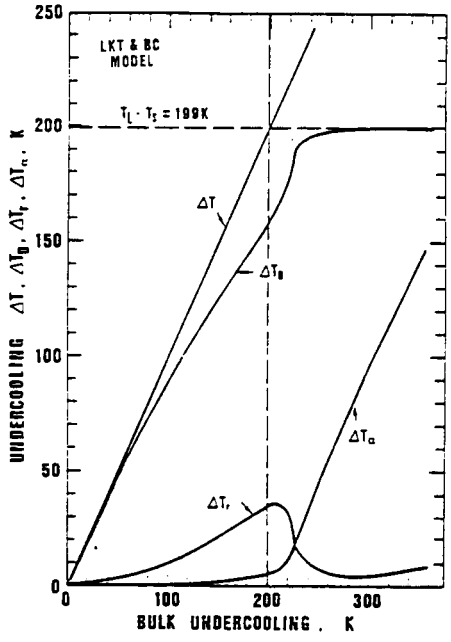

Figure 7. Results of calculations of solutal undercooling (ΔT_D), capillarity undercooling (ΔT_r), and thermal undercooling (ΔT_α) as functions of bulk undercooling, using the Lipton, Kurz, and Trivedi model.

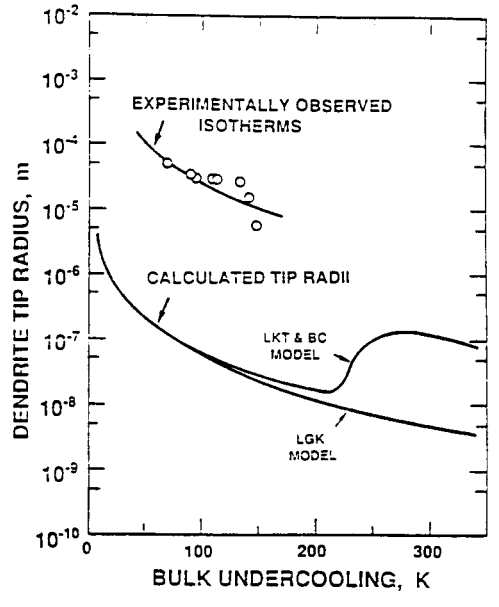

Figure 8. Measured coarse "dendrite" tip radius and calculated dendrite tip radius vs. bulk undercooling for Ni-25wt%Sn alloy.

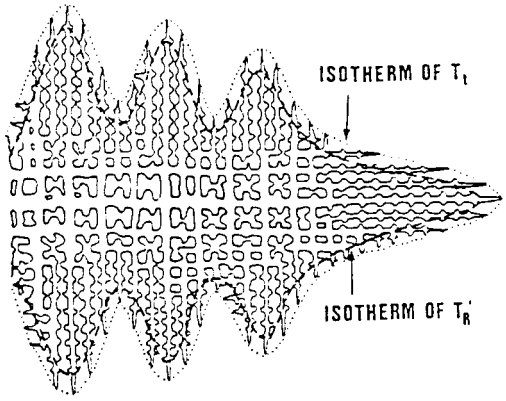

Figure 9. Schematic diagram of coarse "dendrites" growing into undercooled melt.

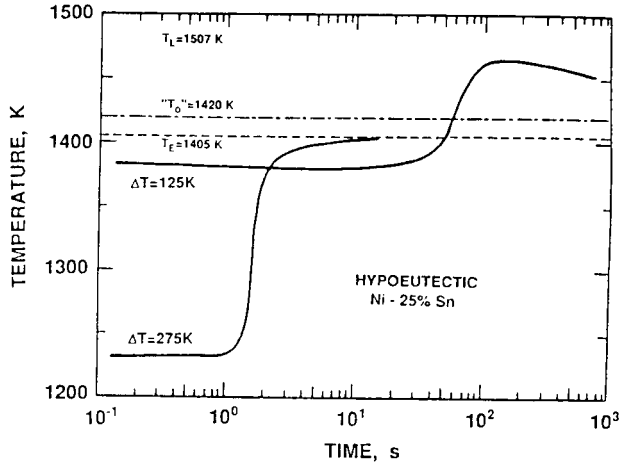

Figure 10. Recalescence behavior of two samples of hypoeutectic alloy. Time scale is logarithmic.

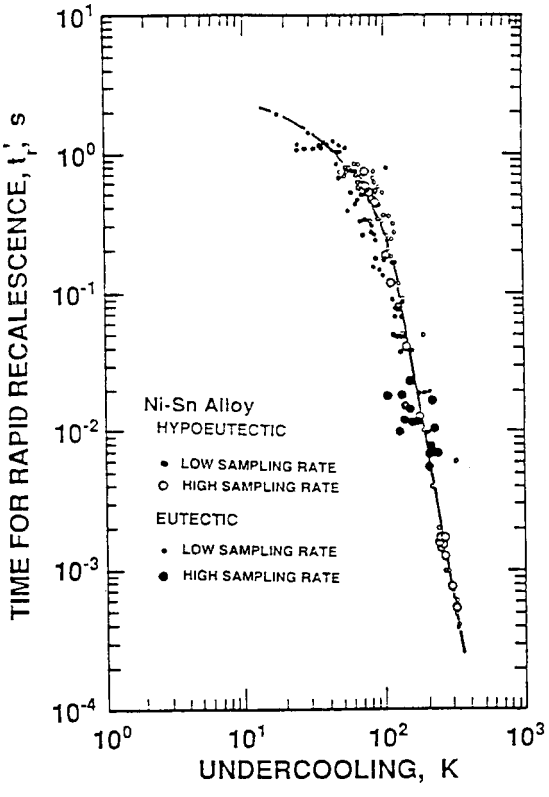

Figure 11. Recalescence time versus undercooling.

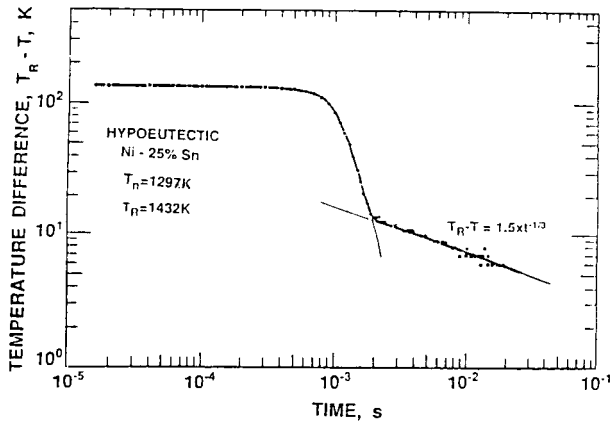

Figure 12. Recalescence behavior, hypoeutectic alloy, plotted on log-log scale to show linear behavior in temperature range of slow recalescence.

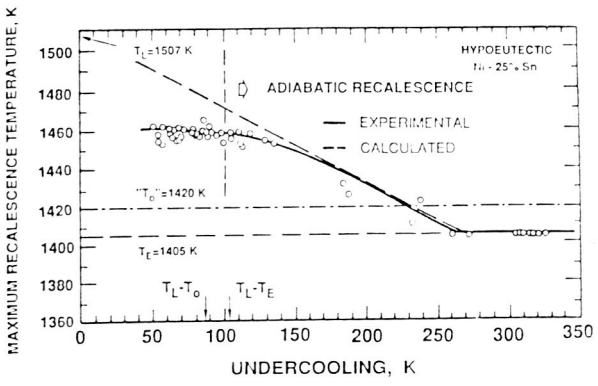

Figure 13. Maximum recalescence temperature, T_R, versus undercooling, hypoeutectic alloy.

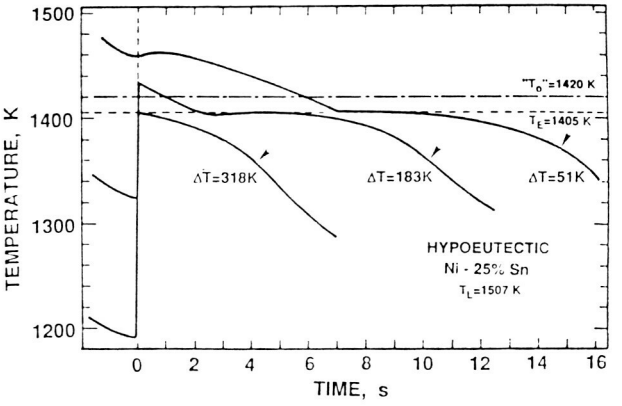

Figure 14. Recalescence and cooling curves for three samples of hypoeutectic alloy, low sampling rate.

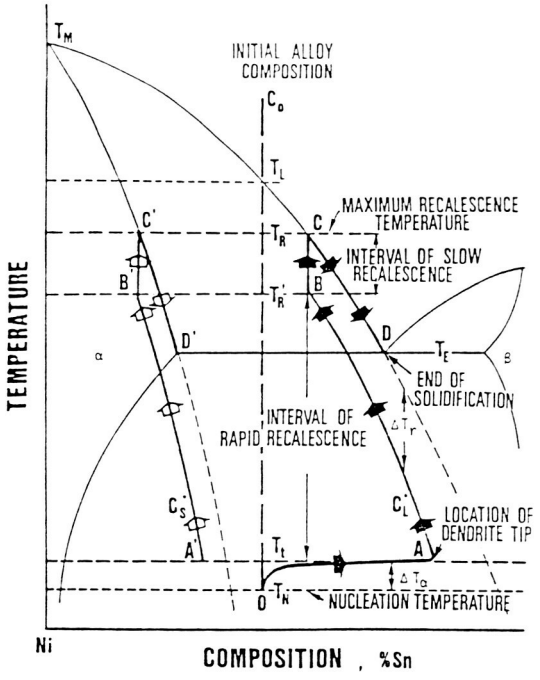

Figure 15. Schematic "solidification path" of undercooled Ni-25wt%Sn alloy. ABCD is the path of the liquid composition at the liquid-solid interface. A'B'C'D' is the path of the solid composition at the liquid-solid interface. Path OA describes the change in solute concentration in front of the advancing dendrite tip. The temperature difference between the two "paths" and the phase diagram extensions are exaggerated.

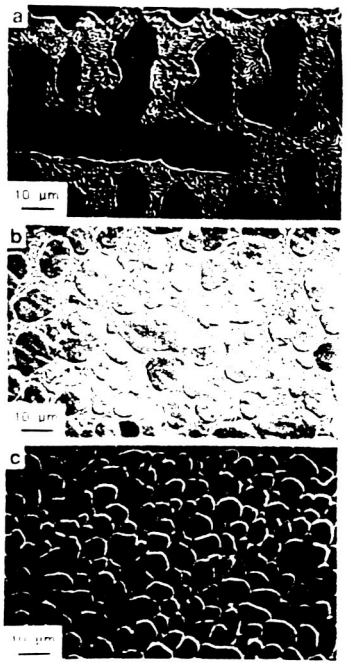

Figure 16. Cross-sectional microstructures of three Ni-25wt%Sn hypoeutectic alloy samples with different initial undercoolings. (a) 112K; (b) 183K; and (c) 324K.

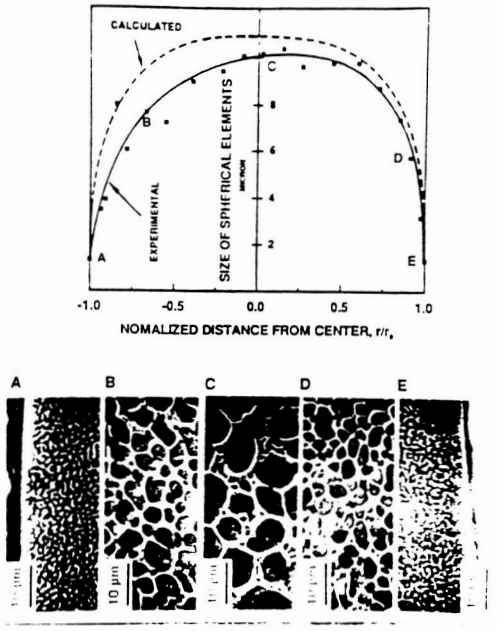

Figure 17. Dependence of diameter of spherical elements on position in a Ni-25wt%Sn hypoeutectic alloy sample undercooled by 324 K. The five photographs correspond to the five data points labeled in the plot.

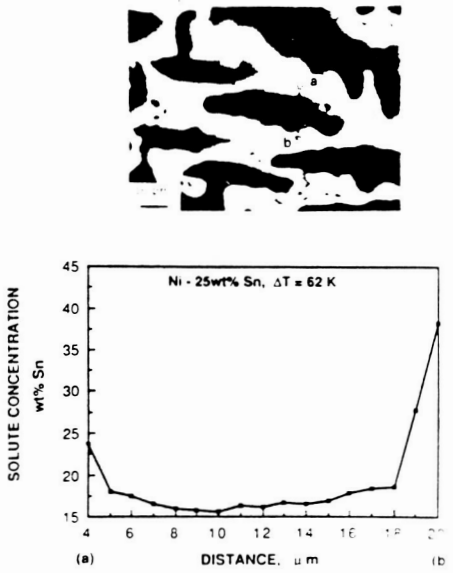

Figure 18. Composition profile across one dendrite arm, measured by electron microprobe, in a Ni-25wtTSn alloy sample undercooled by 62K. Note that the solute-poor core revealed qualitatively by the contrast difference was confirmed by the quantitative measurement.

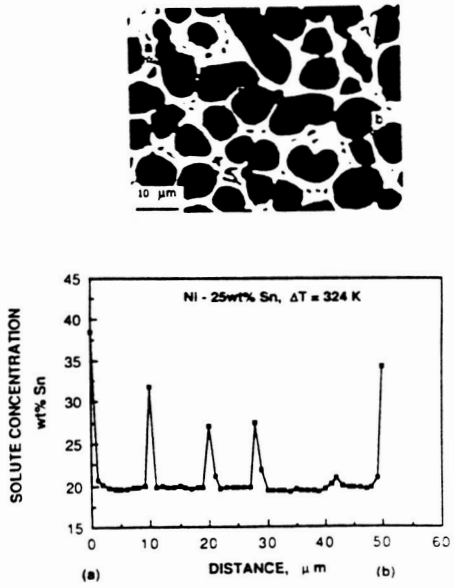

Figure 19. Composition profile across five spherical dendrite elements, measured by electron microprobe, in a Ni-25wt%Sn alloy sample undercooled by 324K. Note that the contrastdifference observed here was not the result of a composition difference.

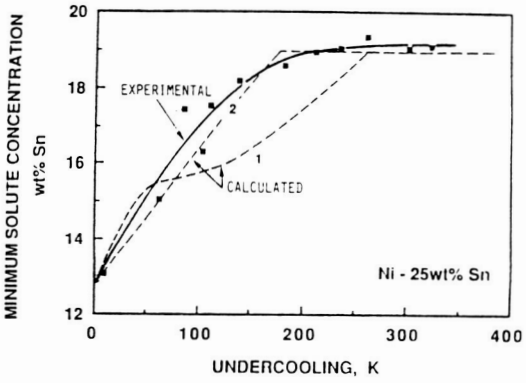

Figure 20. Comparison of experimental results of minimum solute concentration versus undercooling with calculations for Ni-25wt%Sn alloy.

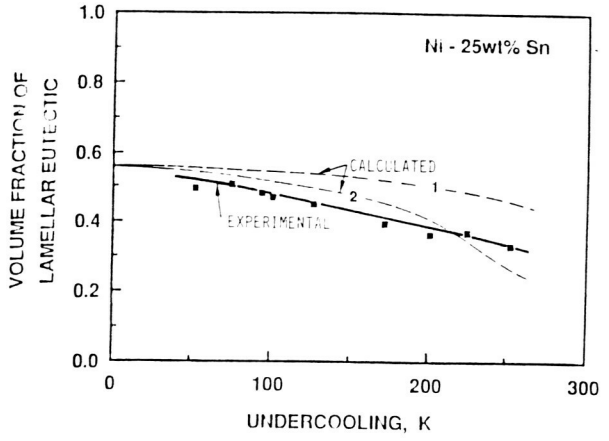

Figure 21. Comparison of experimenatl results of volume fraction of lamellar eutectic structure versus undercooling with calculations for Ni-25wt%Sn alloy.

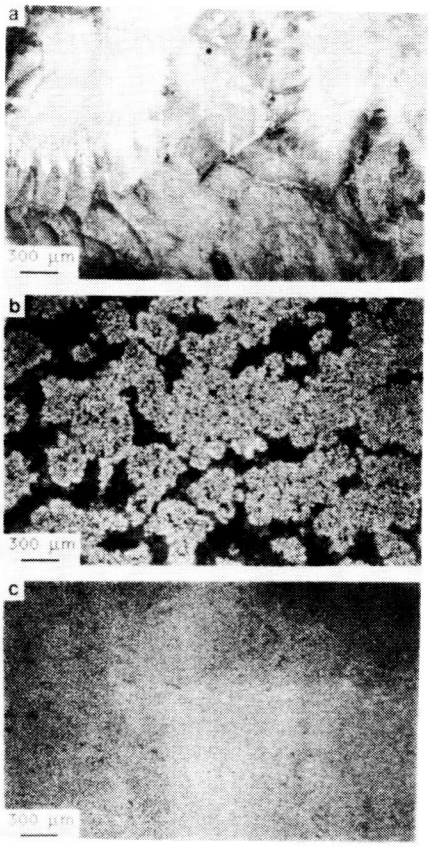

Figure 22. Cross-sectional Microstructures, taken by optical microscopy at low magnification, for three Ni-32.5wt%Sn eutectic alloy samples with different undercoolings, showing the dendrite-like appearance of the anomalous eutectic regions. Undercoolings: (a) 31K; (b) 113K; and (c) 225K.

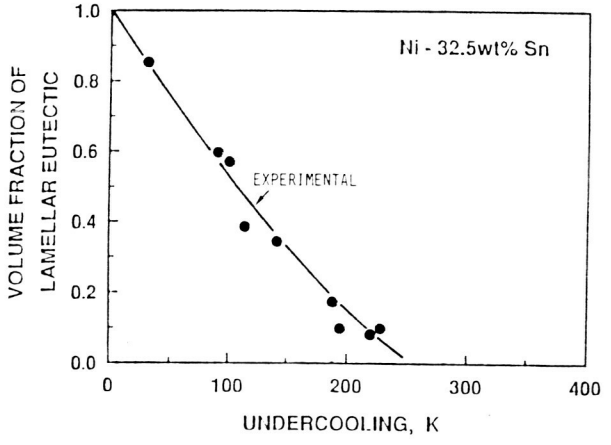

Figure 23. Plot of volume fraction of lamellar eutectic structure versus undercooling for Ni-32.5wt%Sn alloy.

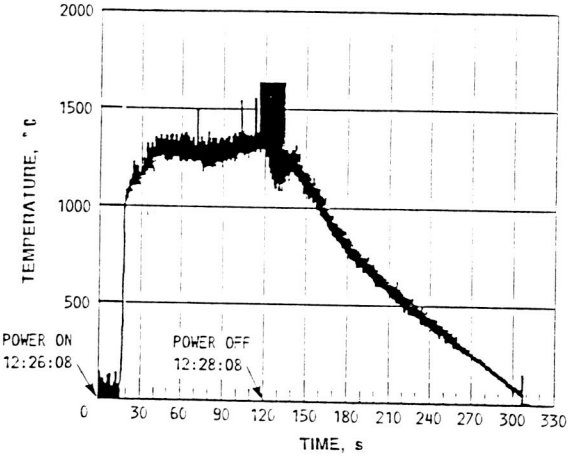

Figure 24. Time-temperature trace of flight specimen during processing, obtained using a pyrometer at 125 measurements per second.

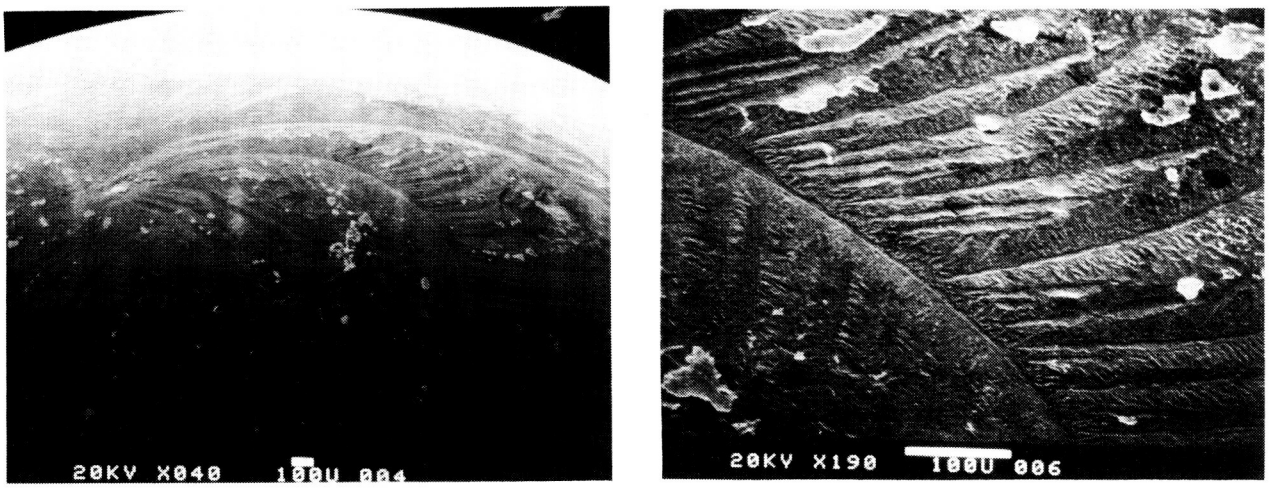

Figure 25. Surface microstructures of flight specimen, showing (a) apparent nucleation site and large curved dendrite, and (b) non-orthogonal secondary dendrite arms.

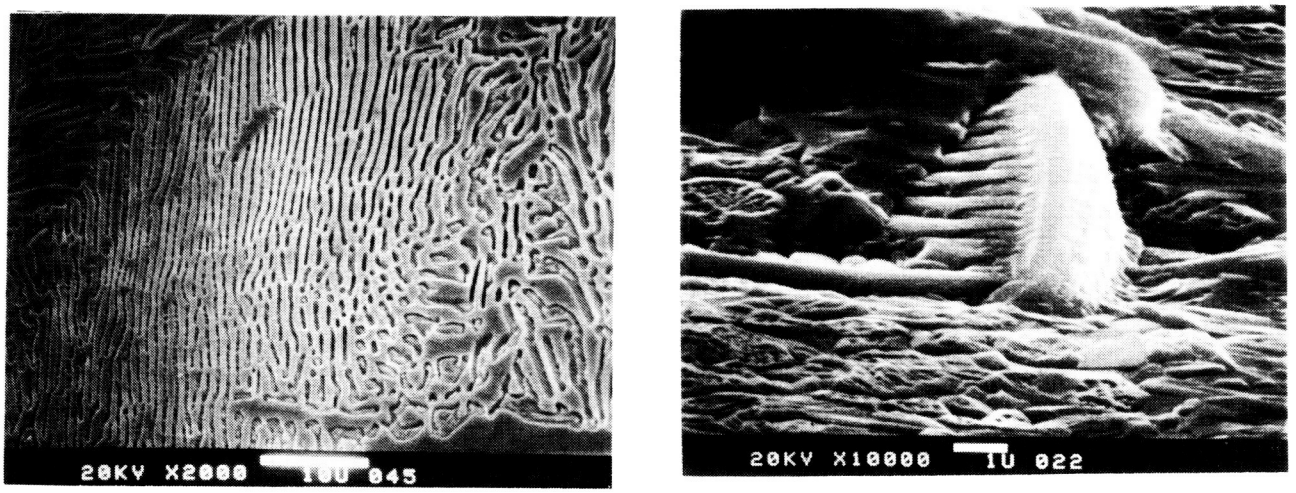

Figure 26. Cross-sectional microstructure of flight specimen, showing lamellar eutectic (left) and anomalous eutectic (right).

Figure 27. Fine dendrite fragment on flight specimen surface.